

Synthesis and self-assembly of Cu_{1.94}S–ZnS heterostructured nanorods†

Luoxin Yi,^a Aiwei Tang,^b Mu Niu,^a Wei Han,^a Yanbing Hou^b and Mingyuan Gao^{*a}

Received 23rd March 2010, Accepted 1st June 2010

DOI: 10.1039/c0ce00026d

Cu_{1.94}S–ZnS heterostructured nanorods are prepared by injecting Zn(acac)₂-dodecanethiol solution into hot reaction systems containing Cu_{1.94}S nanocrystals which catalyze the pyrolysis of Zn(acac)₂ and the following epitaxial growth of ZnS on Cu_{1.94}S seeds. Crystallographic analysis suggests that the built-in p–n type heterostructures allow the dipole moment vectors of both the Cu_{1.94}S “head” and ZnS “tail” to overlap, consequently giving rise to unexpected zipper-like self-assembled structures formed by the heterostructured Cu_{1.94}S–ZnS nanorods.

Introduction

Semiconductor–semiconductor heterostructured nanorods have attracted great research interests owing to their potential applications in many fields, such as photovoltaic devices, high-performance catalysis, and new-generation optoelectronic devices.^{1–3} Until now, two different types of growth modes have successfully been employed in creating heterostructured nanorods, *i.e.*, seeded growth⁴ and catalyst-assisted growth.⁵

In the seeded growth, the heteroepitaxial growth involves the formation of seeds of one material followed by the epitaxial growth of the second material. In general, the growth mechanism of asymmetric binary nanocrystals proceeds through the formation of an as small as possible curved interface as a means to accommodate the high interfacial lattice strain between the two material domains, therefore a limited mutual lattice constant mismatch is the key for constructing binary nanocrystals.^{6,7} Nevertheless, a large interface between two semiconductor materials may persist if the respective lattice constants do not differ significantly, and/or the interface energy remains low throughout the synthesis, which gives rise to a symmetric coating of the second material on the core, forming core/shell type nanocrystals. For instance, the following pairs of II–VI semiconductors such as CdSe–CdS,⁸ CdSe–CdTe,^{9,10} and CdSe–ZnS¹¹ have successfully been used for creating highly fluorescent core/shell type nanocrystals. The growth of semiconductor nanocrystals is very complicated due to the fact that different preparative conditions may lead to different growth mechanisms, *i.e.*, kinetics-dominated and thermal dynamics-dominated growth.¹² Taking II–VI semiconductors as examples, they can form elongated nanocrystals along [001] in an environment with a high chemical potential *via* a kinetics-driven process.¹³ Therefore, judicious adjustment of the synthetic parameters also allows

the formation of II–VI nanoheterostructures with rod and even tetrapod morphologies.^{14,15}

With respect to materials that possess limited mutual compatibility in crystal lattice constants, a small shared interface is likely to form if two domains can find respective facets with small enough mutual lattice mismatches. In such a case, the shared interface needs to be perpendicular to the preferential growth axis of the second material, so as to form a heterostructure with rod morphology.^{6,7} Otherwise, heterodimers or irregular heterostructures, such as FePt–CdS dimers,¹⁶ γ -Fe₂O₃/CdS dimers¹⁷ and Fe₃O₄/CdS¹⁸ anisotropic nanocrystal heterostructures are formed instead of heterostructured nanorods.

An alternative way of creating one-dimensional heterostructures by seeded growth is to use rods rather than dots as seeds by taking advantage of the higher reactivity of the rod tips. Following this route, Au particle-tipped CdSe nanorods,¹⁹ CdS nanorods,²⁰ Co nanorods,²¹ as well as Co particle-tipped TiO₂ nanorods⁷ have been reported. However, in all these systems, particles are often found at both ends of the rods, except for Au–CdSe nanorods.²² The symmetric structure of Au–CdSe–Au only represents an intermediate stage and can transform into a more stable structure with a single Au particle on the tip of CdSe nanorods *via* an “electrochemical intra-rod ripening” process.²² In contrast, with respect to semiconductor–semiconductor systems, dumbbell-like nanorods such as PbSe–CdSe–PbSe,²³ CdTe–CdS–CdTe,²³ CdTe–CdSe–CdTe,²⁴ PbSe–CdS–PbSe,²⁵ and CdS–CdTe–CdS²⁶ are more often formed instead of the asymmetric ones because both ends of the rod-like seeds have similar reactivity, which also applies when dot-like particles are used as seeds.¹⁸

The catalyst-assisted growth presents a number of advantages over seeded growth in synthesizing one-dimensional structures with much larger aspect ratios. The catalyzing mechanisms can be classified as vapor–liquid–solid (VLS),²⁷ solution–liquid–solid (SLS),²⁸ and supercritical-fluid–liquid–solid (SFSL) processes.²⁹ In general, all these mechanisms rely on the use of low melting point nanoparticles as catalysts, which are exclusively chosen from Au, Bi, In, Sn and their alloys so far. Among these mechanisms, SLS, which can be considered as an extension of VLS, has been adopted for producing InP,³⁰ GaAs,³¹ CdSe³² and Si semiconductor nanowires in solution.³³ By further feeding precursors of the second semiconductor material, semiconductor–semiconductor heterostructured nanowires such as

^aInstitute of Chemistry, CAS, Bei Yi Jie 2, Zhong Guan Cun, 100190 Beijing, China. E-mail: gaomy@iccas.ac.cn; Fax: +0086 (0)10 82613214; Tel: +0086 (0)10 82613214

^bKey Laboratory of Luminescence and Optical Information, Ministry of Education, Institute of Optoelectronic Technology, Beijing JiaoTong University, 100044 Beijing, China

† Electronic supplementary information (ESI) available: Synthetic procedures for Cu_{1.94}S–ZnS nanorods and other information. See DOI: 10.1039/c0ce00026d

(Bi)CdS–CdSe³⁴ and (Bi)ZnSe–ZnTe³⁵ can also be synthesized. Governed by the inherent mechanisms, the catalyst-assisted growth is generally more favorable for creating one-dimensional asymmetric semiconductor heterostructures.

Recently, we have for the first time demonstrated that Cu_{1.94}S nanocrystals can also be used as catalysts in synthesizing one-dimensional nanorods of III–VI semiconductors such as In₂S₃, forming matchstick-like Cu₂S–In₂S₃ heterostructures.³⁶ Different from the metal nanoparticle catalysts used in the SLS synthesis, Cu_{2–x}S is a naturally occurring p-type semiconductor and has become one of the best choices for constructing high-performance photovoltaic devices in conjunction with n-type II–VI semiconductors.³⁷ Therefore, it is meaningful to further explore the potential of using Cu_{2–x}S nanoparticles as catalysts in the synthesis of heterostructured nanorods consisting of II–VI semiconductors for achieving new materials of potential use for optoelectronic and photovoltaic applications. ZnS is an important n-type II–VI semiconductor with a direct wide bandgap of 3.91 eV.³⁸ Herein, we report the synthesis and self-assembled structures of Cu_{1.94}S–ZnS heterostructured nanorods.

Experimental

Materials

Copper(II) acetylacetonate [Cu(acac)₂] and zinc(II) acetylacetonate [Zn(acac)₂] were prepared according to literature methods,^{39,40} and used after twice being recrystallized. *n*-Dodecanethiol, and all the other solvents used in the current investigations were commercially available products of analytical grade and used without further purification.

Preparation of Cu_{1.94}S–ZnS heterostructured nanorods

In general, the preparation of Cu_{1.94}S–ZnS nanorods was carried out by a multi-step injection of Zn(acac)₂-dodecanethiol stock solutions into a hot Cu(acac)₂-dodecanethiol reaction system which generated Cu_{1.94}S nanoparticles. To tune the morphology of the resultant Cu_{1.94}S–ZnS nanorods and verify the catalyst-assisted growth mechanism, the injection time of Zn(acac)₂, molar ratio of Zn(acac)₂ : Cu(acac)₂, as well as the reaction time were varied. In detail, 0.13 g (0.5 mmol) of Cu(acac)₂ powder was dispersed in 30 mL of dodecanethiol with the aid of magnetic stirring, and then nitrogen gas was introduced to purge the reaction solution. After ~20 min, the sky-blue mixture obtained was quickly heated to 200 °C within ~20 min in an oil-bath. Then the resultant solution was maintained at 200 °C during the following synthesis. Incidentally, during the increase of temperature, the reaction mixture first changed from turbid blue to turbid white, and then abruptly turned to transparent yellow at around 148–152 °C. These phenomena have been observed previously and are demonstrated to be associated with the formation and decomposition of the Cu–dodecanethiol complex, and the reduction of Cu(II) to monovalent Cu(I) by dodecanethiol.^{36,41} In the meantime, 15 mL dodecanethiol stock solution containing 0.13 g (0.5 mmol) Zn(acac)₂ was prepared and divided into six equal portions which were intermittently injected into the hot Cu(acac)₂-dodecanethiol solution at 200 °C at fixed time intervals. For example, the first portion was injected after Cu(acac)₂ and dodecanethiol reacted for 25 min and the second

portion was followed 20 min later. The remaining four injections were separated by a time interval of 1 h. To tune the morphology of the resultant nanorods, two additional series of samples were prepared with the first injection being carried out after the initial Cu(acac)₂-dodecanethiol system was kept at 200 °C for 43 min and 200 min, respectively. The following intermittent injections were added at the same time intervals to enable direct comparison. More details are provided in Scheme S1 (ESI†). Aliquots were extracted and labeled as *F-R-T* to follow the growth of the nanorods, where *F* (in minutes) stands for the time point where the first portion of Zn(acac)₂ was injected, *R* and *T* designate for the total molar ratio of Zn(acac)₂ : Cu(acac)₂, and the time (in hours) elapsed after the final injection, respectively.

Preparation of zipper-like self-assembled structures

The zipper-like self-assembled structures of the Cu_{1.94}S–ZnS heterostructured nanorods were obtained as follows. A carbon-coated TEM grid was placed in a cold glass vial, and then a tiny drop of toluene solution containing heterostructure nanorods was dripped gently on the grid using a microsyringe. After that, the vial was sealed and stored at 4 °C in refrigerator to let the solvent evaporate as slowly as possible.

Characterization

Low-resolution transmission electron microscopy (TEM) images and selected-area electron diffraction (SAED) patterns were recorded with a JEM-100CXII electron microscope operating at an accelerating voltage of 100 kV. High-resolution TEM (HRTEM) images were taken on FEI Tecnai 20 working at an accelerating voltage of 200 kV. Statistical sizes of the resultant particles were determined by counting more than 300 nanocrystals per sample. Powder X-ray diffraction (XRD) patterns were obtained with a Rigaku D/Max-2500 diffractometer equipped with a Cu-K α_1 radiation ($\lambda = 1.54056$ Å).

Results and discussion

Characterization of Cu_{1.94}S–ZnS heterostructured nanorods

Detailed morphological evolutions of the 25-1-*T* series of samples are presented in Fig. 1. TEM results reveal that the average size of the resultant nanoparticles formed after 25 min of reaction at 200 °C is 13.4 ± 0.9 nm. At this stage, apart from the spherical nanoparticles, sheet-like nanostructures are also present in the system (Fig. 1a), which are formed by coordination polymers constructed by dodecanethiol and Cu(acac)₂.³⁶ After Zn(acac)₂ was completely injected heterostructured nanorods comprised of a spherical “head” and a slightly thinner “stick” were formed (Fig. 1b and c) and grew mainly in length as the reaction was prolonged (Fig. 1d). X-Ray diffraction results in Fig. 1e reveal that the initially formed copper sulfide particles are of Cu_{1.94}S (djurleite, Cu₃₁S₁₆, monoclinic; JCPDS No. 23-0959; $a = 26.897$ Å, $b = 15.745$ Å, $c = 13.565$ Å) and remained unchanged in the binary structures formed later on, while the sticks are of hexagonal ZnS (wurtzite, JCPDS No. 79-2204). Since the strongest diffraction peak of the ZnS phase corresponds to (002) of hexagonal ZnS, the long axis of the nanorods can therefore be identified as the *c* axis of wurtzite ZnS. More

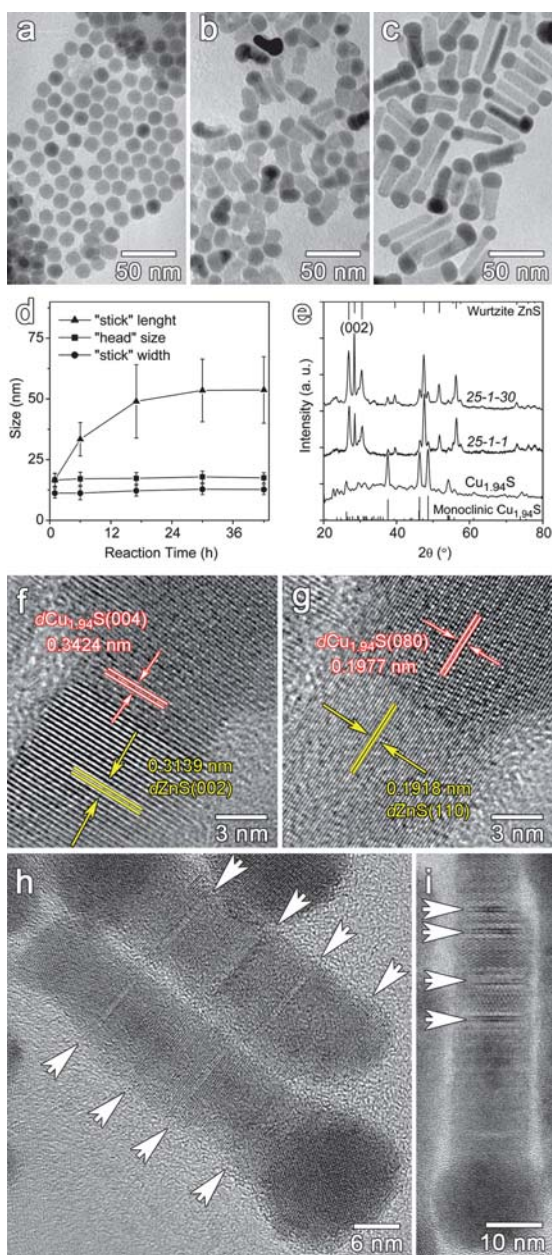


Fig. 1 Panels (a)–(c) present TEM images of copper sulfide nanoparticles obtained after Cu(acac)₂ was pyrolyzed in dodecanethiol at 200 °C for 25 min (a), sample 25-1-1 (b), sample 25-1-6 (c), respectively; panel (d) shows the size evolutions of the 25-1-*T* series of nanorods as a function of *T*; panel (e) provides XRD patterns of the initial copper sulfide nanoparticles and the corresponding nanorods shown in panels (a)–(c), respectively (bottom of the frame: monoclinic Cu_{1.94}S, JCPDS No.23-0959; top of the frame: wurtzite ZnS, JCPDS No. 79-2204); panels (f) and (g) show HRTEM images of two differently oriented heterostructured nanorods overlaid with identifications of crystal planes for both Cu_{1.94}S and ZnS phases; panels (h) and (i) show HRTEM images of nanorods with bamboo-like structures as indicated by white arrows.

detailed interfacial structures of the nanorods were obtained by HRTEM. The results in Fig. 1f and g clearly show that (001)_{Cu_{1.94}S} and (0001)_{ZnS} are parallel to the grain boundary, while (010)_{Cu_{1.94}S} and (11 $\bar{2}$ 0)_{ZnS} are quasi-perpendicular to the

grain boundary. The interface-orientation relationships between the Cu_{1.94}S and ZnS are (010)_{Cu_{1.94}S}|| (11 $\bar{2}$ 0)_{ZnS} and (100)_{Cu_{1.94}S}|| (1 $\bar{1}$ 00)_{ZnS} and the corresponding lattice mismatches are $[d(080) - d(110)]/d(080) \times 100\% = [(0.1959 - 0.1911)/0.1959 \times 100\%] = 2.5\%$ and $[d(800) - d(1\bar{1}0)]/d(800) = [(0.3350 - 0.3311)/0.3350 \times 100\%] = 1.2\%$, respectively. The relatively small lattice mismatches allow the epitaxial growth of hexagonal ZnS on monoclinic Cu_{1.94}S along the *c*-crystallographic axis. Quite interestingly, it was also found out under HRTEM (Fig. 1h) that there exist a number of clear marks across the *c*-axis of ZnS rods, forming a bamboo-like structure in addition to the heterostructure formed by Cu_{1.94}S and ZnS. Such marks are probably caused by the intermittent injections of Zn(acac)₂, as they are moving away from the Cu_{1.94}S “head” upon further growth of the ZnS sticks (Fig. 1i) after all six injections of Zn(acac)₂ were accomplished.

Repetitive nucleation of Cu_{1.94}S induced by Zn(acac)₂

The results shown in Fig. 1a–c further reveal that the monodispersity of the copper sulfide nanoparticles decreases upon the injection of Zn(acac)₂, different from the phenomena observed from the Cu₂S–In₂S₃ system,³⁶ suggesting that repetitive nucleation of Cu_{1.94}S nanocrystals occurred accompanying the growth of ZnS “sticks”. More detailed results on the morphological evolution of the 25-1-*T* series of Cu_{1.94}S–ZnS binary nanocrystals, as shown in Fig. 2, demonstrate that the Cu_{1.94}S “head” size distribution is getting broadened while the “head” is growing bigger. Two size populations develop even before six portions of Zn(acac)₂-dodecanethiol stock solutions was completely injected, which strongly supports that the repetitive nucleation of Cu_{1.94}S nanocrystals occurred during the preparation of 25-1-*T* samples. Due to the formation of a population of smaller Cu_{1.94}S nanocrystals, the overall width distribution of Cu_{1.94}S–ZnS nanorods is bigger than that of the Cu₂S–In₂S₃ nanorods prepared under similar conditions.³⁶

Control over the size and monodispersity of Cu_{1.94}S–ZnS heterostructured nanorods

It was observed that the size of Cu_{1.94}S nanocrystals was a function of the reaction time when solely pyrolyzing Cu(acac)₂ in dodecanethiol. Moreover, the monodispersity of the resultant Cu_{1.94}S remained nearly unchanged as the Cu_{1.94}S nanocrystals are growing larger.³⁶ Therefore, thicker Cu_{1.94}S–ZnS nanorods were expected by postponing the injections of Zn(acac)₂-dodecanethiol stock solutions. For comparison with 25-1-6 (Fig. 1c), 43-1-6 and 200-1-6 were prepared. The TEM results shown in Fig. 3a–d generally support that bigger size of Cu_{1.94}S nanocrystals is in favor of thicker nanorods. Moreover, postponing the injection of Zn(acac)₂ also decreases the width distribution of the resultant Cu_{1.94}S–ZnS nanorods. In the meantime, the difference between the rod width and head size is suppressed. More detailed statistical results are provided in Table 1. These observations can be understood as follows. For the system generating monodispersed Cu_{1.94}S, a burst of nucleation takes place within a very short time window, which is followed by the growth of nucleus without a repetitive nucleation process being involved, supported by the fact that the size distribution of

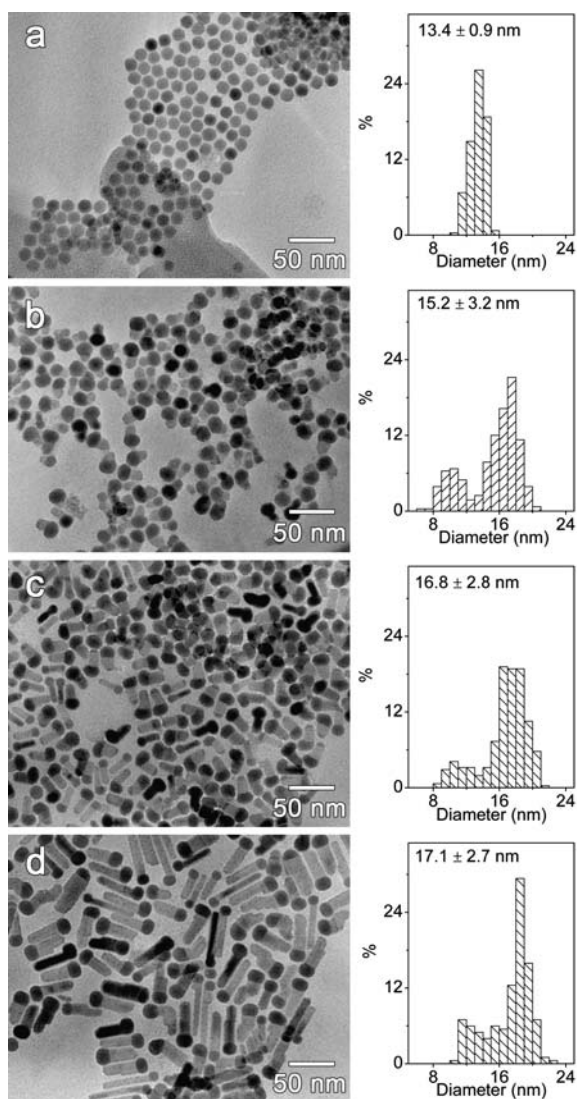


Fig. 2 TEM images of $\text{Cu}_{1.94}\text{S}$ nanocrystals (25 min) (a), 25-1-0* (b), 25-1-1 (c) and 25-1-6 (d), together with the corresponding histograms of the $\text{Cu}_{1.94}\text{S}$ “heads”. (*25-1-0 was extracted just before the final portion of $\text{Zn}(\text{acac})_2$ -dodecanethiol solution was injected).

differently sized $\text{Cu}_{1.94}\text{S}$ nanocrystals remains nearly unchanged vs. reaction time.³⁶ However, the introduction of $\text{Zn}(\text{acac})_2$ greatly disturbs the reaction system, giving rise to repetitive nucleation of $\text{Cu}_{1.94}\text{S}$ while the ZnS phase is formed, consequently the resultant nanorods present increased width distribution as long as the repetitive nucleation is allowed to take place. Nevertheless, as the pyrolysis of $\text{Cu}(\text{acac})_2$ proceeds, $\text{Cu}_{1.94}\text{S}$ nanocrystals grow bigger at the cost of $\text{Cu}(\text{acac})_2$, the repetitive nucleation process is consequently suppressed, leading to the formation of nanorods with a much narrower width distribution.

Because the rod width distributions of 43-1-6 and 200-1-6 are similar but smaller than that of 25-1-6 (see Table 1), it can be deduced that 43 min is long enough to eliminate the repetitive nucleation so as to suppress the width distribution of the resultant nanorods. Therefore, the injection time of 43 min for the first portion of $\text{Zn}(\text{acac})_2$ was fixed for further manipulating the

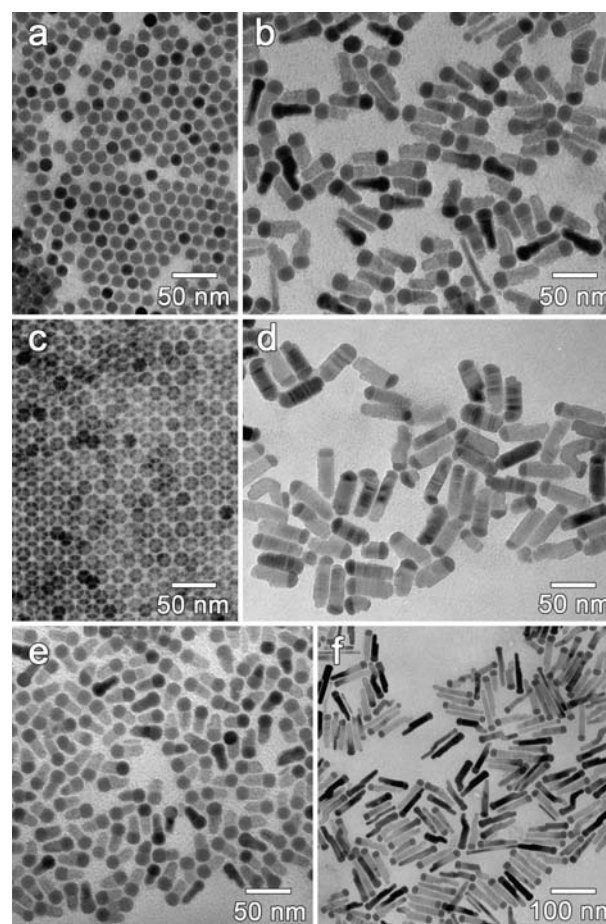


Fig. 3 TEM images of differently sized $\text{Cu}_{1.94}\text{S}$ nanocrystals obtained by pyrolyzing $\text{Cu}(\text{acac})_2$ in dodecanethiol for 43 min (a) and 200 min (c), respectively, together with the resultant $\text{Cu}_{1.94}\text{S}$ -ZnS nanorods samples 43-1-6 (b) and 200-1-6 (d). Panels (e) and (f) show TEM images of samples 43-0.5-6 (e) and sample 43-2-6 (f), respectively.

Table 1 Statistical dimensions (in nm) of F-1-6 series of nanorods and the initial $\text{Cu}_{1.94}\text{S}$ nanocrystals

Sample	Initial $\text{Cu}_{1.94}\text{S}$	$\text{Cu}_{1.94}\text{S}$ in nanorods	ZnS in nanorods (width × length)
25-1-6	13.4 ± 0.9	17.1 ± 2.7	$(11.2 \pm 2.7) \times (33.4 \pm 6.9)$
43-1-6	15.1 ± 1.0	18.1 ± 2.1	$(14.4 \pm 1.9) \times (31.3 \pm 4.9)$
200-1-6	17.9 ± 0.9	18.3 ± 2.1	$(17.4 \pm 2.1) \times (38.0 \pm 5.9)$

length of the heterostructured nanorods by varying the $\text{Zn}(\text{acac})_2$: $\text{Cu}(\text{acac})_2$ ratio. The nanorods shown in Fig. 3e (43-0.5-6) and Fig. 3f (43-2-6) were obtained using $\text{Zn}(\text{acac})_2$: $\text{Cu}(\text{acac})_2$ molar ratios of 0.5 and 2, respectively. Statistical results reveal that the rod width of sample 43-0.5-6 and 43-2-6 are nearly the same, but the rod length is greatly increased by raising the $\text{Zn}(\text{acac})_2$: $\text{Cu}(\text{acac})_2$ ratio.

Formation mechanism of $\text{Cu}_{1.94}\text{S}$ -ZnS heterostructured nanorods

Previous investigations suggest that the $\text{Cu}_{1.94}\text{S}$ nanocrystals can catalyze the formation of In_2S_3 leading to the growth of

heterostructured $\text{Cu}_2\text{S-In}_2\text{S}_3$ nanorods.³⁶ To further verify that catalyst-assisted growth mechanism also applies for the current systems, the following experiment was performed by simultaneously introducing $\text{Cu}(\text{acac})_2$ and $\text{Zn}(\text{acac})_2$ into dodecanethiol before initiating the reaction through heating treatment. The TEM results shown in Fig. 4a reveal that most ZnS nanorods obtained present a quasi-tapered structure with some of them possessing interesting step-like side structures (Fig. 4a and b). More careful observations on single nanorods with step-like side structures reveal that the ZnS “stick” is a perfect single crystal with no defects being present in the vicinity of each step (Fig. 4c and e). As a matter of fact, step-like side structures along the ZnS sticks can also be found from the prepared samples while $\text{Cu}_{1.94}\text{S}$ nanocrystals show a great tendency to grow bigger before the injection of $\text{Zn}(\text{acac})_2$, for example sample 25-1-6 shown in

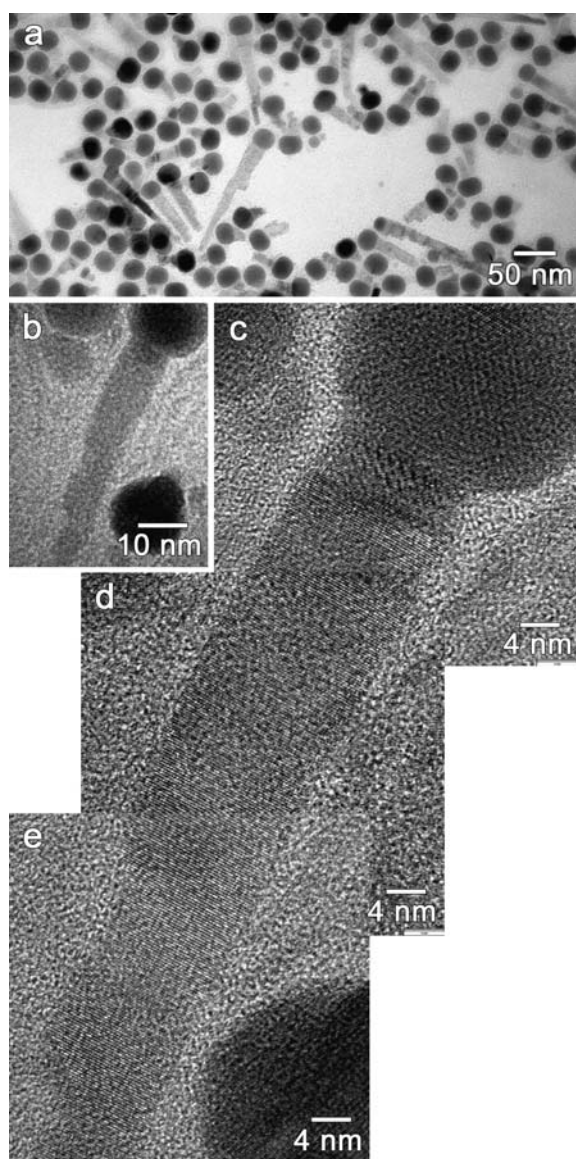


Fig. 4 TEM images (a, b) and HRTEM images (c–e) of the nanocrystals obtained by simultaneously pyrolyzing $\text{Cu}(\text{acac})_2$ and $\text{Zn}(\text{acac})_2$ at 200 °C in dodecanethiol for 17 h. Images (c–e) are the high resolution version of image (b).

Fig. 1c. These structural characteristics suggest that the ZnS phase is formed from the $\text{Cu}_{1.94}\text{S}$ side. As the $\text{Cu}_{1.94}\text{S}$ particles are getting larger, the newly formed ZnS nanorods are consequently getting thicker, giving rise to the taper-like ZnS rods. Because $\text{Zn}(\text{acac})_2$ is rather stable, supported by the fact that no nanoparticles were found after keeping $\text{Zn}(\text{acac})_2$ -dodecanethiol solution at 200 °C for the same period of reaction time, therefore it can be concluded that $\text{Cu}_{1.94}\text{S}$ nanocrystals also serve as catalyst for the formation of the ZnS phase in addition to acting as a growing template for the formation of $\text{Cu}_{1.94}\text{S}$ -ZnS heterostructured nanorods.

Self-assembly of $\text{Cu}_{1.94}\text{S}$ -ZnS heterostructured nanorods

Apart from the unique structural features such as bamboo-like rods as a result of the multi-step injections of $\text{Zn}(\text{acac})_2$ and step-like side structures along the ZnS sticks as a result of the continuous growth of the catalyst particles, the current $\text{Cu}_{1.94}\text{S}$ -ZnS nanorods with proper size also present interesting and quite unexpected zipper-like self-assembled structures. As a matter of fact, the nanorods shown in Fig. 3b (sample 43-1-6) have already shown such a tendency. The TEM sample shown in Fig. 3b was prepared by free-drying a small droplet of a chloroform solution containing sample 43-1-6. To increase the ordering degree, another TEM sample of the same nanorods was prepared by slowing drying the nanorods dispersed in toluene instead of chloroform. The results shown in Fig. 5a and b clearly demonstrate that the $\text{Cu}_{1.94}\text{S}$ -ZnS nanorods possess great a tendency to form zipper-like self-assembled structures. Similar behavior was also observed from sample 25-1-17 with a larger aspect ratio as shown in Fig. 5c. In fact, II–VI semiconductors possess a strong electric dipole moment along the *c*-crystallographic axis. Driven by dipole–dipole interaction, alignments of II–VI nanorods such

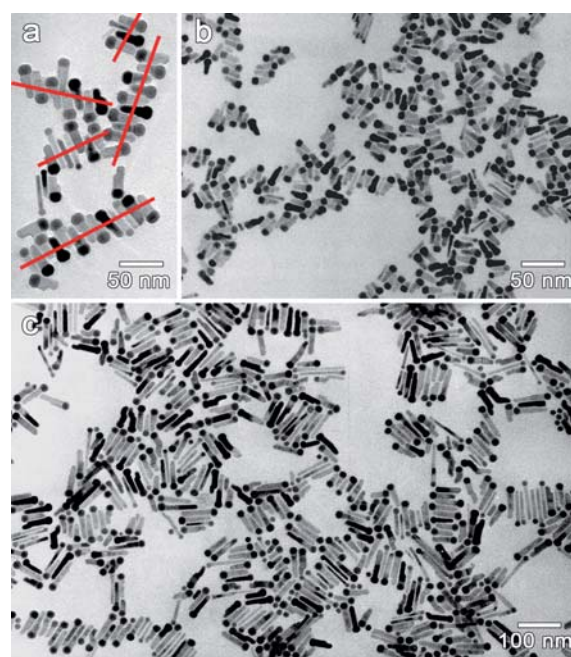


Fig. 5 Zipper-like self-assembled structures formed by samples 43-0.5-6 (a, b) and 25-0.5-17 (c). The red lines are drawn across the self-assembled arrays as a guide to the eye.

as CdSe and CdS have been reported.⁴² In comparison with CdSe and CdS, ZnS however presents a relatively weaker dipole moment.⁴³ Therefore, self-alignment of ZnS nanorods driven by dipole–dipole interaction has rarely been reported. According to the investigations of Alivisatos and co-workers, the longitudinal permanent electric dipole moment of wurtzite nanocrystals increases linearly with volume.⁴⁴ However, no apparently increased ordering degree of the zipper-like self-assembled structures is seen with respect to Cu_{1.94}S–ZnS nanorods with longer ZnS rods (sample 25-1-17 shown in Fig. 5c). Therefore, it can be deduced that the Cu_{1.94}S “head” should also contribute to the electric dipole moment of heterostructured nanorods apart from that of the ZnS “tail”. In fact, monoclinic forms of copper sulfide are ferroelectric, and therefore exhibit a spontaneous electric polarization.⁴⁵ According to theoretical investigations of Talapin and co-workers,⁴⁶ the dipole–dipole interactions among spherical particles also play an important role for forming three-dimensional superlattice structures, which is supported by our experimental observations that an increasing number of three-dimensional self-assembled structures appear as the Cu_{1.94}S nanocrystals grow larger.³⁶ Since the electric dipole moment of hexagonal Cu₂S is along the [001] direction,⁴⁷ as a pseudo-hexagonal crystal, the dipole moment of monoclinic Cu_{1.94}S should also be along the [001] direction, meaning that the electric dipole moment directions of both the Cu_{1.94}S “head” and ZnS “tail” are overlapped. Consequently, the migration of charge carriers across the interface between Cu_{1.94}S and ZnS will greatly enhance the longitudinal electric dipole moment of the Cu_{1.94}S–ZnS nanorods as they hold p–n type heterostructures. Therefore, it can be concluded that the built-in heterostructures induce the formation of zipper-like self-assembled structures *via* electric dipole–dipole interactions.

Conclusions

In summary, Cu_{1.94}S–ZnS heterostructured nanorods are prepared by injecting Zn(acac)₂-dodecanethiol into hot reaction systems containing Cu_{1.94}S nanocrystals. The aspect ratio of the resultant nanorods is demonstrated to be a function of the molar ratio of Zn(acac)₂ and Cu(acac)₂. Higher Zn(acac)₂ : Cu(acac)₂ ratios are found to favor longer nanorods. Crystallographic stacking analysis suggests the built-in p–n type of heterostructures allows the dipole moment vectors of both the Cu_{1.94}S “head” and ZnS “tail” to overlap, consequently giving rise to the interesting zipper-like self-assembled structures formed by the heterostructured Cu_{1.94}S–ZnS nanorods. Further morphological investigations suggest that Cu_{1.94}S nanocrystals catalyze the pyrolysis of subsequently introduced Zn(acac)₂ as well as the epitaxial growth of ZnS along the *c*-crystallographic axis, which leads to the formation of Cu_{1.94}S–ZnS heterostructured nanorods. The current investigations further demonstrate that Cu_{1.94}S particles, as an alternative choice of metal particle catalysts, have great potential for producing interesting one-dimensional semiconductor nanomaterials with remarkable properties.

Acknowledgements

The current investigations were partly supported by NSFC projects (20673128, 20640430564, 20820102035).

Notes and References

- 1 F. Qian, S. Gradecak, Y. Li, C. Y. Wen and C. M. Lieber, *Nano Lett.*, 2005, **5**, 2287.
- 2 H. Zhong, Y. Zhou, Y. Yang, C. Yang and Y. Li, *J. Phys. Chem. C*, 2007, **111**, 6538.
- 3 Y. H. Zheng, L. R. Zheng, Y. Y. Zhan, X. Y. Lin, Q. Zheng and K. M. Wei, *Inorg. Chem.*, 2007, **46**, 6980.
- 4 T. Pellegrino, A. Fiore, E. Carlino, C. Giannini, P. D. Cozzoli, G. Ciccarella, M. Respaud, L. Palmirotta, R. Cingolani and L. Manna, *J. Am. Chem. Soc.*, 2006, **128**, 6690.
- 5 Y. Jung, D. K. Ko and R. Agarwal, *Nano Lett.*, 2007, **7**, 264.
- 6 R. Buonsanti, V. Grillo, E. Carlino, C. Giannini, M. L. Curri, C. Innocenti, C. Sangregorio, K. Achterhold, F. G. Parak, A. Agostiano and P. D. Cozzoli, *J. Am. Chem. Soc.*, 2006, **128**, 16953.
- 7 M. Casavola, V. Grillo, E. Carlino, C. Giannini, F. Gozzo, E. F. Pinel, M. A. Garcia, L. Manna, R. Cingolani and P. D. Cozzoli, *Nano Lett.*, 2007, **7**, 1386.
- 8 L. Carbone, C. Nobile, M. De Giorg, F. D. Sala, G. Morello, P. Pompa, M. Hytch, E. Snoeck, A. Fiore, I. R. Franchini, M. Nadasan, A. F. Silvestre, L. Chiodo, S. Kuder, R. Cingolani, R. Krahne and L. Manna, *Nano Lett.*, 2007, **7**, 2942.
- 9 B. Blackman, D. M. Battaglia, T. D. Mishima, M. B. Johnson and X. G. Peng, *Chem. Mater.*, 2007, **19**, 3815.
- 10 J. E. Halpert, V. J. Porter, J. P. Zimmer and M. G. Bawendi, *J. Am. Chem. Soc.*, 2006, **128**, 12590.
- 11 T. Mokari and U. Banin, *Chem. Mater.*, 2003, **15**, 3955.
- 12 X. G. Peng, *Adv. Mater.*, 2003, **15**, 459.
- 13 Z. A. Peng and X. G. Peng, *J. Am. Chem. Soc.*, 2002, **124**, 3343.
- 14 D. J. Milliron, S. M. Hughes, Y. Cui, L. Manna, J. B. Li, L. W. Wang and A. P. Alivisatos, *Nature*, 2004, **430**, 190.
- 15 R. G. Xie, U. Kolb and T. Basche, *Small*, 2006, **2**, 1454.
- 16 H. W. Gu, R. K. Zheng, X. X. Zhang and B. Xu, *J. Am. Chem. Soc.*, 2004, **126**, 5664.
- 17 K. W. Kwon and M. Shim, *J. Am. Chem. Soc.*, 2005, **127**, 10269.
- 18 H. McDaniel and M. Shim, *ACS Nano*, 2009, **3**, 434.
- 19 T. Mokari, E. Rothenberg, I. Popov, R. Costi and U. Banin, *Science*, 2004, **304**, 1787.
- 20 A. E. Saunders, I. Popov and U. Banin, *J. Phys. Chem. B*, 2006, **110**, 25421.
- 21 T. Wetz, K. Soulantica, A. Talqui, M. Respaud, E. Snoeck and B. Chaudret, *Angew. Chem., Int. Ed.*, 2007, **46**, 7079.
- 22 T. Mokari, C. G. Sztrum, A. Salant, E. Rabani and U. Banin, *Nat. Mater.*, 2005, **4**, 855.
- 23 L. Carbone, S. Kuder, C. Giannini, G. Ciccarella, R. Cingolani, P. D. Cozzoli and L. Manna, *J. Mater. Chem.*, 2006, **16**, 3952.
- 24 S. Kumar, M. Jones, S. S. Lo and G. D. Scholes, *Small*, 2007, **3**, 1633.
- 25 S. Kuder, L. Carbone, M. F. Casula, R. Cingolani, A. Falqui, E. Snoeck, W. J. Parak and L. Manna, *Nano Lett.*, 2005, **5**, 445.
- 26 F. Shieh, A. E. Saunders and B. A. Korgel, *J. Phys. Chem. B*, 2005, **109**, 8538.
- 27 Y. Y. Wu and P. D. Yang, *J. Am. Chem. Soc.*, 2001, **123**, 3165.
- 28 T. J. Trentler, K. M. Hickman, S. C. Goel, A. M. Viano, P. C. Gibbons and W. E. Buhro, *Science*, 1995, **270**, 1791.
- 29 J. D. Holmes, K. P. Johnston, R. C. Doty and B. A. Korgel, *Science*, 2000, **287**, 1471.
- 30 F. D. Wang, A. G. Dong, J. W. Sun, R. Tang, H. Yu and W. E. Buhro, *Inorg. Chem.*, 2006, **45**, 7511.
- 31 H. Yu and W. E. Buhro, *Adv. Mater.*, 2003, **15**, 416.
- 32 J. W. Grebinski, K. L. Hull, J. Zhang, T. H. Kosel and M. Kuno, *Chem. Mater.*, 2004, **16**, 5260.
- 33 A. T. Heitsch, D. D. Fanfair, H. Y. Tuan and B. A. Korgel, *J. Am. Chem. Soc.*, 2008, **130**, 5436.
- 34 L. Ouyang, K. N. Maher, C. L. Yu, J. McCarty and H. Park, *J. Am. Chem. Soc.*, 2007, **129**, 133.
- 35 A. G. Dong, F. D. Wang, T. L. Daulton and W. E. Buhro, *Nano Lett.*, 2007, **7**, 1308.
- 36 W. Han, L. Yi, N. Zhao, A. Tang, M. Gao and Z. Tang, *J. Am. Chem. Soc.*, 2008, **130**, 13152.
- 37 A. Ashour, *J. Optoelectron. Adv. Mater.*, 2006, **8**, 1447.
- 38 J. H. Yu, J. Joo, H. M. Park, S. I. Baik, Y. W. Kim, S. C. Kim and T. Hyeon, *J. Am. Chem. Soc.*, 2005, **127**, 5662.
- 39 E. W. Berg and J. E. Strasser, *Anal. Chem.*, 1955, **27**, 127.
- 40 G. Rudolph and M. C. Henry, *Inorg. Chem.*, 1964, **3**, 1317.

-
- 41 T. Kuzuya, Y. Tai, S. Yamamuro and K. Sumiyama, *Sci. Technol. Adv. Mater.*, 2005, **6**, 84–90.
- 42 D. V. Talapin, E. V. Shevchenko, C. B. Murray, A. Kornowski, S. Forster and H. Weller, *J. Am. Chem. Soc.*, 2004, **126**, 12984.
- 43 S. G. Raptis, M. G. Papadopoulos and A. J. Sadlej, *J. Chem. Phys.*, 1999, **111**, 7904.
- 44 L. S. Li and A. P. Alivisatos, *Phys. Rev. Lett.*, 2003, **90**, 09702–1.
- 45 C. E. Corry, *J. Appl. Geophys.*, 1994, **32**, 55.
- 46 D. V. Talapin, E. V. Shevchenko, C. B. Murray, A. V. Titov and P. Kral, *Nano Lett.*, 2007, **7**, 1213.
- 47 Z. Zhuang, Q. Peng, B. Zhang and Y. Li, *J. Am. Chem. Soc.*, 2008, **130**, 10482.